IEEE Access
Multidisciplinary | Rapid Review | Open Access Journal

Date of publication xxxx 00, 0000, date of current version xxxx 00, 0000.

Digital Object Identifier 10.1109/ACCESS.2024.0429000

A Novel Digital Twin – based Framework and Methodology for Enhancing the Contribution of Loads to Frequency Control

JESÚS ARAÚZ[1], ANTOINE LABONNE[1], YVON BESANGER[1],(Senior Member, IEEE), FRÉDERIC WURTZ[1],(Member, IEEE), SIMON WACZOWICZ[2], VEIT HAGENMEYER[2],

[1]Univ. Grenoble Alpes, CNRS, Grenoble INP, G2Elab, Grenoble, 38000, France (e-mail: jesus-harmodio.arauz-sarmiento@grenoble-inp.fr, antoine.labonne@grenoble-inp.fr, Yvon.Besanger@g2elab.grenoble-inp.fr, frederic.wurtz@g2elab.grenoble-inp.fr)
[2]Karlsruhe Institute of Technology, Institute for Automation and Applied Informatics, Kaiserstraße 12, Karlsruhe, 76131, Germany (e-mail: simon.waczowicz@kit.edu, veit.hagenmeyer@kit.edu)

Corresponding author: Jesús Araúz (e-mail: jesus-harmodio.arauz-sarmiento@grenoble-inp.fr).

This research was partly funded by the IRGA Foundation of Université Grenoble Alpes, by the French National Research Agency in the framework of the "Investissements d'avenir" program (ANR-15-IDEX-02), and the Helmholtz Association of German Research Centres (HGF) within the framework of the Program-Oriented Funding POF IV in the program Energy Systems Design (ESD, project numbers 37.12.01, 37.12.02, and 37.12.03).

ABSTRACT The integration of renewable energy sources into power grids is crucial for reducing carbon emissions, yet it introduces challenges related to frequency stability due to reduced inertia and renewable intermittency. Although many solutions have been explored, the role of loads in frequency control remains underdeveloped. This work presents a novel Digital Twin framework for frequency control, incorporating six load frequency control schemes implemented on a thermal load. Additionally, it proposes a methodology for constructing frequency-control-oriented Digital Twins of power systems. The framework uses real-time measurements to estimate grid parameters—via the swing equation—and continuously tune control gains for enhanced performance. Complementarily, an online inertia estimation technique is integrated to enable fully adaptive strategies, further improving frequency control. The proposed approach is validated through computational and Hardware-in-the-Loop experimentation, showing robust performance under real-world conditions such as measurement noise and delays. The results indicate that integrating Digital Twins with load-based frequency control significantly enhances the power system's resilience, offering a promising direction for future improvements in grid stability.

INDEX TERMS Demand response, Digital Twins, Frequency control, Hardware-in-the-Loop, Machine learning, Methodology, Thermal loads.

I. INTRODUCTION

Addressing Climate Change requires an energy transition, including tripling renewable energy capacity and doubling efficiency by 2030 [1]. Achieving high renewable generation (RG) penetration demands deeper electricity sector decarbonization, posing two main challenges [2]: cost-effective demand supply and a reliable grid with high converter-interface generation (CIG) [3]. This necessitates further research on converter design, control, and grid integration.

It is well-known that increasing the presence of CIG in grids involves new challenges. The normal behavior of the power system is changing due to intermittent RG, such as in wind turbines (WT) and photovoltaic (PV) plants, and high penetration of power electronics [4]. Power electronics are present not only in CIG but in modern loads, energy storage systems (ESS) [5], and transmission devices. Integrating a large share of these devices requires redefining the stability of the power system [6].

One of the most affected stability issues is frequency control. Since CIG does not have rotating masses, or any other intrinsic means to provide inertia, power systems are becoming more vulnerable to uncertainties and power disturbances, associated with classical and, especially, modern power systems [7]. Therefore, dealing with these updated power system stability types [6] is extremely necessary to achieve 100% RG-based consumption.

Nomenclature

Acronyms

BESS	Baterry storage system
CIG	Converter-interface generation
CIL	Converter-interfaced load
DER	Distributed energy resource
DR	Demand response
DT	Digital twin
ESS	Energy storage system
EV	Electric vehicle
FCP	Frequency control proposal
HIL	Hardware-in-the-Loop
HVAC	Heating, ventilation, and air conditioning
LAN	Local area network
LFC	Load frequency control
LR	Linear regression
LS	Least square
ML	Machine learning
MPC	Model predictive control
OIE	Online inertia estimation
OLS	Ordinary least square
pbs	probing signal
PFC	Primary frequency control
PHIL	Power Hardware-in-the-Loop
PV	Photovoltaic
RG	Renewable generation
RL	Reinforcement learning
RMS	Root mean square
RoCoF	Rate of change of frequency
SFC	Secondary frequency control
SG	Synchronous generator
SOC	State of charge
VI	Virtual inertia
VPP	Virtual power plant
WT	Wind turbines

Parameters

η	HVAC system efficiency
A_{ji}	Heat transfer area related to i^{th} and j^{th} thermal systems in m^2
C_i	Thermal capacity of the i^{th} thermal system in kJ/ °C
C_{droop}	Generic droop coefficient
$D_i(s)$	Generator dynamics transfer function
D_{eq}	Equivalent power system damping
K_{Load}^{PFC}	Fixed primary frequency control gain
K_{Load}^{SFC}	Fixed secondary frequency control gain
K_{Load}^{VI}	Fixed virtual inertia frequency control gain
U_{ji}	Heat transfer coefficient related to i^{th} and j^{th} thermal systems in $kW/m^2/$°C

Subscripts

adj	adjusted
d	discriminant
eq	equivalent
exp	expected
i	i^{th} generator or thermal subsystem
inj	injected
j	i^{th} thermal subsystem
set	setpoint

Variables

$\Delta f(s)$	Frequency deviation in p.u.
$\Delta P_{Load}(s)$	Load power deviation in p.u.
$\dot{m}$	HVAC system mass flow in Kg/s
E	Load step amplitude in p.u.
$G(s)$	Generators combined (dynamics and controllers) transfer function
H_{eq}	Equivalent system inertia coefficient in seconds
$i(t)$	Generic time-dependent input signal
$K_{exp,real}^{PFC}$	Primary frequency control gain, expected and real
$K_{exp,real}^{SFC}$	Secondary frequency control gain, expected and real
$K_{exp,real}^{VI}$	Virtual inertia frequency control gain, expected and real
$o(t)$	Generic time-dependent output signal
P_{HVAC}	HVAC system electric power in kW
Q_j	j^{th} heat gain in kW
Q_{HVAC}	HVAC system heat gain in kW
r	Ratio between frequency control gains
T_i	i^{th} thermal system temperature in °C
T_j	j^{th} thermal system temperature in °C
T_{inj}	Injected air temperature in °C
T_{set}	Setpoint temperature in °C
T_{zone}	zone temperature in °C

II. LITERATURE REVIEW

From an overall perspective, many research works have been conducted to maintain stability in low-inertia power systems. Most frequency control techniques can be classified into three categories: from a generation perspective, from a transmission perspective, and from a load perspective. The difference in results obtained among these categories is noticeable. The generation and transmission perspectives have been investigated more thoroughly than the one from the load perspective [7].

From the generation and transmission perspective, numerous works on conventional synchronous generators (SGs), PV, WT, transmission devices, and ESS can be found. Some of them addressed the modification of the standard PV controller to provide primary frequency control (PFC) and virtual inertia (VI), with/without ESS support [8]. Other authors proposed a virtual power plant (VPP) approach to optimize the coordinated response of ESS, PV, and loads to provide frequency control [9]. The authors of [10] chose WT to supply over 80% of the electricity consumption of Ireland, with well-known frequency control techniques for RG and battery ESS to achieve dispatchable generation and avoid frequency instability. In addition to providing frequency control capacity to RG, many authors have focused on reducing uncertainties by combining frequency control techniques with forecasting methods, commonly based on machine learning (ML) algorithms [11].

As noted in [7], little research has been done on the contribution of the demand side to frequency control. However, some authors have provided solutions for ancillary services, mainly frequency control, from loads. In [12] an architecture for providing frequency and voltage control for electric vehicles (EV) is proposed. The charge/discharge of electric vehicles is regulated through the dynamics of the distribution grid. In [13] and [14] also EV fleets are considered, but they are controlled as VPP or dispatchable consumption to smooth power fluctuation from WT and increase revenues based on ancillary service prices. In [15], an aluminum smelter, fed through a HVDC link, is included in a VPP based on model predictive control (MPC) to reduce frequency deviation in the

provision of secondary frequency control.

In reality, transportation and industry are not the biggest electricity consumers, but buildings [16]. In buildings, the highest consumption comes from thermal processes, such as heating, ventilation, and air conditioning (HVAC) systems, refrigerators, freezers, and hot water production. Taking this into account, building and/or thermal loads have a great potential to contribute to the increase in the penetration of RG into power system [17].

Some authors have tested the reliability and resulting benefits of using HVAC systems, and similar systems as refrigerators, to provide frequency control [18]–[22]. The extent of benefits depends on many parameters, such as nominal power, size of systems, interoperability of controllers, access to hardware/software modifications, etc. [19]. However, all results demonstrated the effectiveness of the thermal load contribution. HVAC systems' effectiveness for frequency control has led to adapted control schemes for train HVACs, enabling railway contributions to grid stability [23], [24] without compromising train operations or requiring additional PV/WT support [25]–[27].

As noted earlier, the benefits of demand response (DR) depend on numerous hard-to-model loads. The energy transition alters RG and SG penetration, shifting grid dynamics. Prior studies emphasized the difficulty of controller tuning under high stochasticity [26]. While adaptive controllers can leverage expected-vs-real-time condition margins [28], they still require a non-changing system model.

Many authors, in various applications, have proposed methodologies based on the Digital-Twin (DT) concept—a synchronized digital counterpart of a physical system that continuously updates and interacts with it in real-time. Such a virtual replica enables enhanced load support for power systems [29].

DT-based methodologies have recently been included as an alternative to deal with power system stability-related questions [30]. In [31], a DT of a battery ESS (BESS) is proposed to forecast the State of Charge (SOC) and to improve the BESS contribution to frequency control. In [32], a DT of a BESS is proposed for contributing to frequency control, damping control, and WT-based power fluctuation mitigation. In [33] a DT-based coordinated frequency control strategy for distributed energy resources (DERs) is proposed, where each DER uses the DT of the others DERs. Similarly in [34], [35], the DT of DERs are implemented in energy management strategies to optimize the RE and ESS resources in microgrids. In [36] a DT-based distribution grid model is implemented for planning and operational decisions. In [37], a Power Hardware-in-the-Loop (PHIL) approach is employed to assess the impact of real DERs on a microgrid using a DT of the system.

Most of these works created DT based on data-driven approaches, such as implementing ML or Reinforcement Learning (RL) techniques. All these works used DT for optimization, forecasting, and planning. However, the expected DT capacity to be updated in real-time has not been demonstrated. Some works, such as [33] and [38], did state this specific characteristic, but did not yet implement and validate that requirement. Furthermore, most of the works about the use of DT for power system stability do not consider the possible contribution of loads. Less related works considered loads but not in power systems [39], [40].

To address the identified research gap concerning the underexplored role of controllable loads in frequency control, and the limited application of DT methodologies on the demand side for such tasks, this work proposes a novel DT-based frequency control framework for loads. The main contributions of this work are summarized as follows:

- The identification and formalization of a research gap regarding the limited exploration of controllable loads and the application of DT methodologies in load-side frequency control.
- The introduction of a novel framework that integrates a power system DT into load-side frequency control schemes.
- The development of an ML-based approach to create and continuously update the power system DT.
- The design of two general frequency control schemes, encompassing PFC, Secondary Frequency Control (SFC), VI services.
- The implementation and evaluation of the proposed framework on two types of loads: an idealized controllable load and a realistic HVAC system.

The paper is structured as follows: Section III covers the methodology for power system DT modeling, loads, HVAC systems, and frequency control schemes. Section IV evaluates the proposed methods through case studies and experiments. Finally, Section V presents key findings, conclusions, and future research directions.

III. METHODS

The proposed DT-based frequency control framework requires taking into account the dynamics of the power system and its DT, the controllable load, and the implementation of the frequency controllers.

A. POWER SYSTEM DIGITAL TWIN

While extensive power system modeling resources exist—from conventional components [41] to power electronics [42], including detailed SG dynamics [43] and excitation systems [44]—not all are essential. Required dynamics depend on study objectives [45]. Also, using highly detailed models, along with numerous online measurements, may increase the DT complexity and the implementation of its self-updating capacity.

As noted in the reviewed works, the development of load frequency control (LFC) models for frequency control studies is sufficient and appropriate, since it reduces the need to manage multiple variables and parameters while accurately representing the frequency behavior. This modeling methodology is based on the well-known swing equation. This can

be represented as (1) in *per unit* (p.u.). Here, s is the Laplace operator; $\Delta f(s)$ is the frequency deviation; $\Delta P_{Load}(s)$ is the load power deviation; H_{eq} is the equivalent system inertia coefficient; D_{eq} is the equivalent system damping coefficient; and $G_i(s)$ is the combined transfer function of the i^{th} generator, in a system with n generators, that represents the effect of transient dynamics, speed controllers, and the presence in the power dispatch. Equation (1) also shows the low-inertia condition of a power system with high penetration of CIG. Under the same frequency control schemes, less H_{eq}, due to the displacement of SG, provides larger frequency deviations.

$$\Delta f(s) = \frac{-\Delta P_{Load}(s)}{2H_{eq}s + D_{eq} + \sum_{i=1}^{n} G_i(s)} \tag{1}$$

Therefore, a frequency-oriented DT is proposed, based on (1). The implementation of DT requires the real values of every term of (1). The frequency and load deviation can be measured in real time. However, H_{eq} and D_{eq} are constantly changing in power dispatch. Additionally, depending on the power system under study, it is often challenging to know the dynamics and controllers of the generators, $\sum_{i=1}^{n} G_i(s)$.

If the DT is deployed in a well-known grid (e.g., industrial networks, small-scale grids, etc.), it is possible to update the DT depending on the status of each generator and consumer. For this, a physics-based DT would be enough. However, this would be a challenge in large-scale grids with a high penetration of DERs. As noted in the literature, data-driven approaches can be an option to deal with high-complexity dynamics. A practical DT implementation can combine the strengths of data-driven models and the physics-based formulation in (1), following a gray-box modeling approach. In this case, (1) defines the general dynamic structure, while the data are used to tune or adapt the parameters to match the observed system behavior.

Equation (2) is derived from (1) to evidence the linear relation among (1) terms. Depending on the objectives and available resources, some terms, such as D_{eq} and $\sum_{i=1}^{n} G_i(s)$, can be neglected or simplified.

$$\begin{aligned}(2H_{eq})\ s\Delta f(s) + (D_{eq})\ \Delta f(s) + \\ \left(\sum_{i=1}^{n} G_i(s)\right)\ \Delta f(s) = -\Delta P_{Load}(s)\end{aligned} \tag{2}$$

Many authors have proposed several online inertia estimation (OIE) methods to solve this problem. In [46], a linear least squares (LS) optimization technique is used during transients to estimate inertia, damping, and mechanical power. In [47], the inertia is estimated using LS optimization, the vector fitting technique, and a testing signal. In [48], a linear regression (LR) method and a testing signal are used to estimate inertia and damping. In [49], the inertia is estimated using an energy-based approach under high-noise and load events. In [50], an LR method is implemented to estimate inertia, power variants, and rotor speed. In [51], the inertia and equivalent time constants of the PFC are estimated using LS optimization.

Following the need to improve the frequency control provision from loads, (2) can be adjusted to track the variation of inertia and damping. Using it, it is possible to modify certain frequency control schemes from loads, such as [24]. Additionally, the present work proposes to expand the implementation to also track changes in the equivalent integral gain of the equivalent power system controller scheme, $\sum_{i=1}^{n} G_i(s)$.

As is known, the SG common controller scheme includes gains proportional to the frequency deviation and its cumulative [41]. The contribution to system inertia is intrinsically due to the electromagnetic coupling. CIG must include schemes, such as the ones in [24], [26], to provide the same type of frequency control. The equivalent controllers of all power system generators can be expressed simply as in (3) [27]. For this, the generator dynamics, $D_i(s)$, affects the gain, K, of each frequency control loop.

$$\sum_{i=1}^{n} G_i(s) = \sum_{i=1}^{n} \left(K_i^{PFC} + K_i^{VI} s + \frac{K_i^{SFC}}{s}\right) D_i(s) \tag{3}$$

The combination of (2) and (3) exposes a simplified expression to link the frequency-oriented characteristics of every generator to the power system frequency behavior (4). Additionally, (4) highlights the inverse relationships between inertia (both real and virtual) and the rate of change of frequency (RoCoF), between K_i^{PFC} gains and frequency deviations, and between K_i^{SFC} gains and the cumulative frequency deviations. As mentioned in some reviewed works, having derivative terms can make the model highly sensitive to noise. Therefore, as an alternative to introduce filtering stages, an extended integral form can be implemented (5).

$$\begin{aligned}\left(2H_{eq} + \sum_{i=1}^{n} K_i^{VI} D_i(s)\right) s\Delta f(s) + \\ \left(D_{eq} + \sum_{i=1}^{n} K_i^{PFC} D_i(s)\right) \Delta f(s) + \\ \left(\sum_{i=1}^{n} K_i^{SFC} D_i(s)\right) \frac{\Delta f(s)}{s} = -\Delta P_{Load}(s)\end{aligned} \tag{4}$$

$$\begin{aligned}\left(2H_{eq} + \sum_{i=1}^{n} K_i^{VI} D_i(s)\right) \Delta f(s) + \\ \left(D_{eq} + \sum_{i=1}^{n} K_i^{PFC} D_i(s)\right) \frac{\Delta f(s)}{s} + \\ \left(\sum_{i=1}^{n} K_i^{SFC} D_i(s)\right) \frac{\Delta f(s)}{s^2} = \frac{-\Delta P_{Load}(s)}{s}\end{aligned} \tag{5}$$

Equation (5) can be arranged to evidence the linear problem formulation, $\mathbf{A(s)} \cdot \mathbf{X(s)} = \mathbf{B(s)}$, as shown in (6). Here, $\mathbf{A(s)}$ is the matrix of coefficients, $\mathbf{X(s)}$ is the vector of variables, and $\mathbf{B(s)}$ is the vector of independent terms.

$$\underbrace{\begin{bmatrix} 2H_{eq} + \sum_{i=1}^{n} K_i^{VI} D_i(s) \\ D_{eq} + \sum_{i=1}^{n} K_i^{PFC} D_i(s) \\ \sum_{i=1}^{n} K_i^{SFC} D_i(s) \end{bmatrix}^{\top}}_{\mathbf{A}(s)} \cdot \underbrace{\begin{bmatrix} \Delta f(s) \\ \frac{\Delta f(s)}{s} \\ \frac{\Delta f(s)}{s^2} \end{bmatrix}}_{\mathbf{X}(s)} = \underbrace{\frac{-\Delta P_{Load}(s)}{s}}_{\mathbf{B}(s)} \tag{6}$$

To simplify the solution of $\mathbf{A(s)}$, certain adjustments may be made. As noted in some reviewed works, the term $D_i(s)$ can be neglected depending on the level of penetration of generation technologies (e.g., under high levels of CIG). It can also be neglected if the frequency of power deviations is outside the band of $\sum_{i=1}^{n} D_i(s)$. This can be regulated by the appropriate selection of a probing signal [52].

Hence, the first term of $\mathbf{A(s)}$ would represent the instantaneous equivalent inertia coefficient, K_{eq}^{VI}. H_{eq} is set by the SGs, but $\sum_{i=1}^{n} K_i^{VI}(s)$ would be the equivalent effect of all CIG and DR loads that provide VI frequency control. The second term of $\mathbf{A(s)}$ would normally be set by the PFC of all generators and DR loads , K_{eq}^{PFC}. As mentioned in the literature, D_{eq} tends to be neglected compared to the effect of $\sum_{i=1}^{n} K_i^{PFC}(s)$. The last term of $\mathbf{A(s)}$ would be established by the contribution to the SFC of all generators and DR loads, K_{eq}^{SFC}. Applying (6) to the previous context and operating in the time domain, (7) is obtained.

$$\underbrace{K_{eq}^{VI} \Delta f(t)}_{A_1 X_1} + \underbrace{K_{eq}^{PFC} \int \Delta f(t)\, dt}_{A_2 X_2} + \underbrace{K_{eq}^{SFC} \int \left(\int \Delta f(t)\, dt \right) dt}_{A_3 X_3} = \underbrace{- \int \Delta P_{Load}(t)\, dt}_{B_1} \tag{7}$$

Equation (7) allows for direct real-time implementation. For example, an ordinary LS (OLS) can be set $\mathbf{A} = \mathbf{X} \backslash \mathbf{B^T}$ in programming languages. Depending on the duration of the probing signal and the sampling rate [48], [52], the number of recorded samples and the execution rate of the OLS is adjusted to the synchronized relation between $\Delta f(t)$ and $\Delta P_{Load}(t)$.

B. LOAD SIDE REPRESENTATION

The loads may interact with the system through the terms $\Delta P_{Load}(s)$ or $\sum_{i=1}^{n} G_i(s)$ (1). From a mathematical perspective, if a load varies over time and its consumption is not influenced by frequency behavior, it affects through $\Delta P_{Load}(s)$. Load events, such as load sheddings, are also included in $\Delta P_{Load}(s)$. If a load is sensitive to frequency behavior, it may be included in $\sum_{i=1}^{n} G_i(s)$. Currently, there is extensive literature on load modeling [53], as well as on assessing the frequency sensitivity of loads [54].

In addition to providing frequency control, loads can contribute to the deployment of DT-based techniques, such as the concepts of Section III-A. As a probing signal may be required, it is proposed to use converter-interfaced loads (CIL), such as the current high-efficiency thermo-fluidic systems (e.g., novel HVAC systems), to establish it. In the literature, this is a task for CIG. The realization of probing signals could be done directly or through an auxiliary ESS. The probing amplitude and frequency depend on the power system characteristics. The amplitude should be enough to cause detectable frequency deviations. The frequency should consider the frequency response of the power system. Detailed examination of the selection of it can be done [46], [48]. However, if the range of grid parameters is known, it may be enough to set one that works for most possible scenarios.

1) Controllable thermal load modeling

Thermal loads are one of the most scattered, relevant, and increasing consumption in power systems (e.g., HVAC systems, refrigerators, and district heating, among others) [16]. This fact makes them an appropriate option for providing multiple services to grids. As mentioned, there is extensive research on thermal load modeling, control, and provision of ancillary services [18]–[27]. From an overall implementation perspective, these models can be divided into two subsystems: the zone to be thermally controlled and the device or system that accomplishes the control. The dynamics of the zone can be simplified into an overall unidimensional and lumped-model expression (8) for a system of k subsystems (i.e., walls, roof, floor, etc.). Here, C_i is the thermal capacity, which is mainly defined by the mass and the specific heat of the i^{th} subsystem; T_i is the temperature of the i^{th} subsystem, as well as T_j of the j^{th} one; $U_{ji}A_{ji}$ is the product of the heat transfer coefficient and the related area of the j^{th} and i^{th} subsystems; and $\dot{Q}_j$ is the j^{th} heat gain in a system with l heat gains (e.g., filtration, radiation through windows, occupancy-related heat, etc.). Equation (8) should be properly managed to introduce specific dynamics, time-variant characteristics, and any other particular requirement.

$$\frac{1}{C_i} \frac{dT_i}{dt} = \sum_{j=1}^{k} U_{ji} A_{ji} \left(T_j - T_i \right) + \sum_{j=1}^{l} \dot{Q}_j \tag{8}$$

On the other hand, the system in charge of controlling a desired T_i, such as an HVAC system, can be modeled in numerous ways, depending on its technology [19]. Equation (9) shows a simplified function to represent the HVAC heat power, $\dot{Q}_{HVAC}$, and its equivalent in electric power, P_{HVAC}, as a function of mass flow ($\dot{m}$), setpoint temperature (T_{set}), injected air temperature (T_{inj}), and zone temperature (T_{zone}). The equivalence between thermal and electric power can be determined using an efficiency coefficient, $\eta(t)$, which can vary over time. It is worth mentioning that T_{zone} is defined by the results of (8), and T_{set}, T_{inj}, and $\dot{m}$ depends on control schemes and other system dynamics (ducts and piping responses; fans and pumps; valves and diffusers; and heat exchangers, among others.). Hence, for more detailed implementations, (8) can be applied to describe the behavior of the terms of (9) in an HVAC system.

$$\dot{Q}_{HVAC}(t) = \eta(t) P_{HVAC}(t) = f\left(\dot{m}, T_{set}, T_{inj}, T_{zone}\right) \quad (9)$$

Numerous works on frequency control from HVAC systems [23]–[27] have modeled (8) with $k = 2$ and (9) as proportional to $\dot{m}\left(T_{set} - T_{zone}\right)$ for cooling mode.

2) Frequency Control

Most CILs tend to adapt the classic frequency control schemes to their controllers. As noted in the literature, HVAC systems are generally considered to provide PFC. Few works implemented VI and SFC. However, the basis of these schemes is the well-known droop control. Equation (10) shows the structure of a classic droop control scheme where $o(t)$ is the output signal, $i(t)$ is the input signal, and C_{droop} is the droop coefficient that modifies the input signal according to an established rate between signal domains.

$$o(t) = C_{droop} * i(t) \quad \text{where} \quad C_{droop} = \frac{\max(o)}{\max(i)} \quad (10)$$

As mentioned in section II, the benefits of frequency control schemes depend on many hard-to-determine and/or changing characteristics. For example, the maximum of $i(t)$, the frequency deviation for PFC, can be defined by (1). In an ideal situation, the only unknown parameter is $\Delta P_{Load}(s)$, but it is still possible to predict certain load deviations and event magnitudes. In real-life situations, as stated in Section III-A, H_{eq} and $G_i(s)$ change over time. Then, not only does the frequency deviation vary over time, but also its extrema and oscillatory behavior. To avoid this challenge, it is common to set $\max(i)$, in (10), according to the grid codes [45]. This results in setting unrealistic maxima that make the droop coefficients small and, therefore, limit the contribution to frequency control.

To face this challenge and take into account the discussion in Section II, two general frequency control schemes for PFC, VI, and SFC are proposed. As introduced in section III-A, a DT-based solution can be implemented to track the changes of inertia and controllers gains (3). The first general scheme is shown in (11). The subscripts *exp* and *real* stand for "expected" and "real-time". This is the ratio ($r^{PFC,\ VI,\ \text{or}\ SFC}$) between expected and real-time gains. This allows to increase the load controller gains $\left(K^{PFC}_{Load},\ K^{VI}_{Load},\ \text{and}\ K^{SFC}_{Load}\right)$ if the power system experiences a decrease of any of them (e.g., during a generator loss).

$$G_{Load}(t) = r^{PFC}\, K^{PFC}_{Load}\, \Delta f(t) + r^{VI}\, K^{VI}_{Load}\, \frac{d\Delta f(t)}{dt} + r^{SFC} K^{SFC}_{Load} \int \Delta f(t)\, dt$$
$$\text{where} \quad r^{PFC} = \frac{K^{PFC}_{exp}}{K^{PFC}_{real}},\ r^{VI} = \frac{K^{VI}_{exp}}{K^{VI}_{real}},\ r^{SFC} = \frac{K^{SFC}_{exp}}{K^{SFC}_{real}} \quad (11)$$

For implementing (11), a well-established starting point is required. It could be at the beginning of the daily energy dispatch, and a very stable situation with information about all the generators, among other possibilities. The second general scheme is based on predicting the maximum frequency deviation, frequency variation, and cumulative frequency deviation to calculate more realistic gains for PFC, VI, and SFC, respectively. This may be done by solving (1) and (3), utilizing the estimations of (7), and assuming a load event type. Equation (12) is derived considering a load step of amplitude E.

$$\Delta f(s) = \frac{-E/s}{K^{VI}_{eq} s + K^{PFC}_{eq} + \frac{K^{SFC}_{eq}}{s}} \quad (12)$$

Equation (12) could be solved analytically, by means of the inverse Laplace transformation, or numerically, using well-known methods for solving differential equations, such as Euler or Heun methods [55]. For example, if (12) is solved by the inverse Laplace transformation, (13) is obtained. This has been performed using the *ilaplace* function from the *specfunc* library, compatible with the TI-*n*spire CX CAS calculator by Texas Instruments®. Alternatively, the same operation can be carried out using the *ilaplace* function provided by the Symbolic Math Toolbox™ in MATLAB. For this, $K^{VI}_{adj} = H_{eq} + \sum_{i=1}^{n} K^{VI}_{i}$ in (6).

$$\Delta f(t) = \frac{E}{C_d}\left(e^{\frac{K^{PFC}_{eq} - C_d}{4K^{VI}_{adj}}t} - e^{\frac{K^{PFC}_{eq} + C_d}{4K^{VI}_{adj}}t}\right)$$
$$\text{where} \quad C_d = \sqrt{8K^{VI}_{adj}K^{SFC}_{eq} + \left(K^{PFC}_{eq}\right)^2} \quad (13)$$

Once instantaneous expression of the frequency deviation is obtained, it is possible to determine its maximum value, as well as the maximum RoCoF and maximum cumulative frequency deviation to establish the droop coefficients (10) for PFC, VI, and SFC, respectively, or any other adjustment. For example, the maximum frequency deviation to calculate the droop of PFC in [23] would be around 0.13 Hz, instead of 0.8 Hz. Therefore, the HVAC system PFC would have performed better.

C. HOLISTIC EXPERIMENTAL VALIDATION

As noted, implementing the proposals implies considering different domains and time scales. In the literature, proposals on frequency control from loads tend to be simplified toward a deeper analysis of the theoretical foundations [23]–[25]. Other works included Hardware-in-the-Loop (HIL) validation, considering external microcontrollers [26]. Some works, such as [27], implemented PHIL where a real generator interacts with an emulated railway system. These kinds of validation are required to test control proposals under close-to-reality conditions. Besides using real controllers, the system to be analyzed and/or controlled should be modeled as realistically and holistically as possible.

As detailed in [56], validations can range from computational simulation to real-scale experimentation. For the intended level of technological readiness of the present work proposals, a first- and second-quadrant validation is sufficient

[56]. Due to the multiphysics and asynchronous nature (frequency deviations, thermal behavior, various time steps, etc.), using several HIL environments is required to approach the intrinsic heterogeneous structure of the proposals. Additionally, multi-HIL device testing can increase the interoperability of the proposals. This approach reduces the need for real-scale experimentation while still addressing some of its most representative challenges, mainly those related to noise and delays, within a well-controlled test bench.

The results of the first quadrant (i.e., computational simulation) and the second quadrant (i.e., real-time HIL experimentation) should be compared. Plotting both groups of curves together may lead to biased conclusions. In contrast to simulations, tests with multiple HILs are not synchronized, and identical conditions from one test to another cannot be ensured, among other implications. Hence, the frequency trajectory over time can be different, providing distinct results. Although the degree of the benefit can differ, the improvement trend should remain [27]. To face this challenge, the use of statistical metrics is proposed. Previous works, such as [24], [27], assessed various frequency control schemes through many statistics. However, the main conclusions are obtained by analyzing Δf. Thus, the performance of the individual scheme and its comparison with others is determined by the root mean square (RMS) of the frequency deviation and the maximum of the absolute frequency deviation, $\max(|\Delta f|)$.

Fig. 1 summarizes the general concept of the proposals (i.e., the integration of the DT of a power system directly into the control scheme of the load) and the experimental implementation selected using two HIL devices. The upper side, related to Section III-A, is deployed in the HIL 1, sends one analog signal to the HIL 2 (lower side, related to Section III-B), and receives two analog signals from the latter. As mentioned in Section III-B, numerous ML-based procedures and models of loads can be used. As a generalized illustration, $f_1(\Delta f)$, $f_2(\Delta f)$, and $f_3(\Delta f)$ represent any signal based on frequency deviation (e.g. derivative, filtered double derivative, etc.). In addition to using any selected probing signal (*Pbs*), any frequency control and setpoint can also be set by the Digital Twin implementation. For this, $[K_{eq}]_{3x1}$ is a representative matrix that collects the estimated power system coefficients that may be used for frequency control. For computational validation, the same interactions occur, but in the same simulation environment.

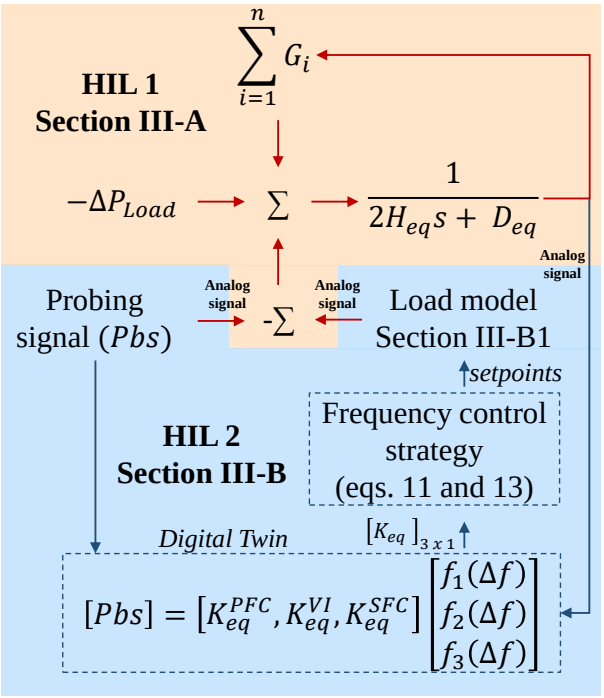

FIGURE 1. Generalized scheme of concept, and modeling of systems and HIL validation: interaction of systems described in Sections III-A and III-B. The orange zone is the power system side. The blue zone is the load side. The color of the arrows represents the zone objective of signals.

IV. CASE STUDY IMPLEMENTATION

Toward the assessment of the implementation of a power system DT into the frequency control of a load, several tests are carried out. The power system is modeled as a LFC scheme two-generator system. The speed controllers have proportional and integral gains of 20 and 0.7, respectively. The inertia of both generators is 11 seconds [41]. The power system experiences a 0.2 p.u. sudden load shedding, followed by a loss of one of the generators, and another 0.2 p.u. load shedding.

The load is modeled in two ways. Firstly, the ideal load, for the overall concept test, consumes power linearly proportional to the frequency deviation, its derivative, and cumulative, following the schemes in (3),(10), and (11). Here, the power setpoint is the real consumed power, as tested in [21], [24]. The second way is as an HVAC system. The zone model, and the HVAC mode operation and the heat-to-electric power ratio, are adapted from [23]–[27]. Therefore, it represents the thermal dynamics of a five-wagon train. There are two main intentions for this model selection. First, it contributes to the expansion of frequency control from railways. Second, it would validate the DT framework and frequency control schemes in low thermal inertia conditions. As seen in the literature, most works rely on the large thermal inertia of the buildings. However, trains are more thermally sensitive than buildings. Therefore, the results would suggest that the proposals are most likely to perform well in almost any thermal system. Previous works on the contribution of railways to frequency control tasks have largely evidenced the

negligible negative impact on thermal comfort [23]–[27].

As commented in Section III-B, the probing signal is iteratively tuned and set to a sinusoidal wave with a frequency and amplitude of 1 rad/s and 0.007 p.u., respectively. The procedure takes into account the main characteristics of the system, such as its natural frequency, response time, and frequency response. When the probing signal is applied, the resulting frequency deviation should ideally exhibit minimal attenuation and phase shift. Otherwise, the LR would estimate inaccurate parameters or slightly biased parameters, depending on the degree of signal attenuation. The amplitude is selected to generate frequency variations that are noticeable by all the participants contributing to the definition of (1). This configuration is expected to be effective across a range of system parameters, including inertia and controller gains. Consequently, the number of observations used for every OLS is obtained as a division between the period of the probing signal and the selected time step. For real-time implementation, the time step should be carefully selected to avoid overruns. Additionally, an appropriate probing signal enables neglecting prime mover dynamics and minimizes bias from specific transients, leading to more generalizable insights.

In contrast to the works cited, the HVAC system is a second-order model that describes the dynamics of the refrigerant and injected air. The model is adapted from [57]. The zone setpoint temperature is controlled by two proportional-integral controllers that modulate air and refrigerant flows. The proportional and integral gains are set to 2.5 and 0.06, respectively. The setpoint temperature is set as one of the frequency control schemes described in Section III-B2. The setpoint temperature modification range is $\pm 2.5\,^{\circ}\mathrm{C}$ and the whole power of the controllable load (i.e., the equivalent HVAC system) is limited to 0.14 p.u., as well as the ideal load. T_{set} (9) is derived from the power obtained by Section III-B2 and scaled to temperature by setpoint temperature and power limits.

It is worth mentioning that dynamic relevance depends on modeling detail. As in Section III-A, using (1) (p.u.) focuses on power proportions and system interactions, avoiding rated power definitions—though this restricts model/parameter choices. This approach simplifies frequency analysis, load/generator scaling, and model aggregation, but requires classic sizing criteria [41] for test stability.

A. COMPUTATIONAL SIMULATIONS

Matlab/Simulink is used for straightforward validation. The power system and loads model, as well as the DT, are implemented directly by the equations shown in Section III. The time step and differential equation solver are 15 milliseconds and Bogacki-Shampine, respectively.

Fig. 2 shows the frequency control performance of an ideal load that supports frequency control tasks according to (3) and defines the gains with (10). The control schemes considered are denoted by the acronym PVS. It represents the first letter of each possible control to be included: PFC, VI, and SFC. The black dashed line represents the reference case, PVS = 000, where the load does not provide frequency control. The frequency ripple is the effect of the probing signal over time. At $t < 400\ s$, the ripple is around 1 mHz. After the generator loss, it is around 2 mHz. The dead band is 0.1 Hz for all cases.

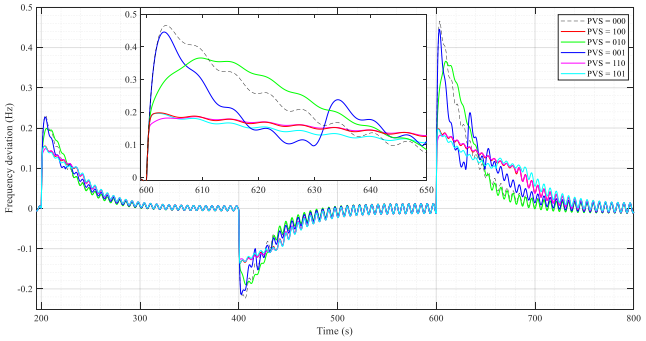

FIGURE 2. Frequency control performance under different events. Control based on (10)**.**

Toward reducing transients and complexity, in the following tests, as well as in Fig. 2, the probing signal is permanently activated. For real and/or specific deployments, the probing signal may be launched when decided. At first glance, it is clear that the combined controls (i.e., PVS = 110 and 101) provide the best performance, followed by a standalone PFC (i.e., PVS = 100). Table 1 shows the RMS and the maximum (max) absolute value of Δf. Both metrics show how the PFC impacts frequency performance the most, while VI and SFC complement. In each table, **bold** numbers represent the best metric result.

TABLE 1. Performance metrics (mHz) of the curves of Fig. 2.

PVS Configuration	Metrics	
	RMS(Δf)	Max($\lvert\Delta f\rvert$)
PVS = 000	73.5755	465.809
PVS = 100	56.8854	197.918
PVS = 010	72.7465	365.976
PVS = 001	66.6801	445.490
PVS = 110	56.8670	**186.085**
PVS = 101	**55.3376**	196.472

The following sections are intended to test the DT-based frequency control rather than delve into the construction of DTs. Also, it is important to test how uncertainty-sensitive the proposals are since they depend on many non-trivial dynamics. As noted in the literature, depending on the objectives, the degree of algorithm development should be adjusted. Sections IV-A1 and IV-A2 expose the impact of DT modeling on frequency control performance. As seen in Fig. 3, accurate tracking of the most representative power system coefficients depends on the methods. Under the same events of Fig. 2, it is evident that using the LR form of (5) (Lr = 1) provides a more stable response under transients than using the LR form of (4) (Lr = 0). At Lr = 0, the estimation is largely affected by the frequency evolution, contrary to at Lr = 1. Both online

estimation scenarios have rate limiters to reduce the impact of noise. The perfect tracking is denoted as Pt.

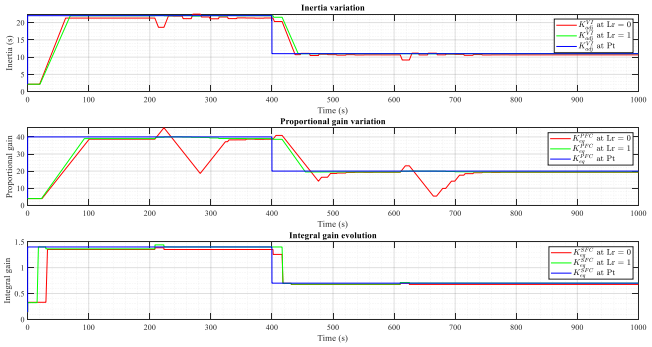

FIGURE 3. Variation of the power system coefficients depending on the DT implementation.

1) Impact of the linear regression implementation on frequency control performance

The present section evaluates the degree of impact of the selection of LR methods for creating the DT. Fig. 4 and Fig. 5 show the frequency evolution under the same events as Fig. 2. Fig. 4 implements a frequency control based on (11), which compensates for the lack of inertia and/or gains over time, and Fig. 5 implements a frequency control based on (13), which calculates the real frequency maxima. The four digits of the legends represent the use of the LR method (Lr = 0 or 1) and the frequency control scheme.

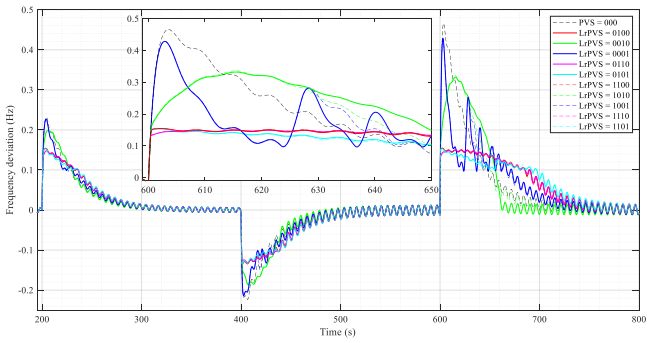

FIGURE 4. Frequency control performance under different events. Comparison between LR implementations. Control based on (11)**.**

At first glance, it is noticeable how the colored dashed lines (Lr = 1) coincide almost perfectly with continuous lines (Lr = 0). According to Table 2, the difference between the metrics at Lr = 1 vs. Lr = 0 is negligible. The greatest differences can be observed in the standalone VI control (PVS = 010), but still around 3 % and 1 % for RMS(Δf) and max($|\Delta f|$), respectively, in the results of Fig. 4. For the results of Fig. 5, the discrepancies are even more negligible. In any case, the uncertainties due to the LR implementation do not represent a relevant impact on frequency control performance. The frequency control based on 13, in addition to performing the best

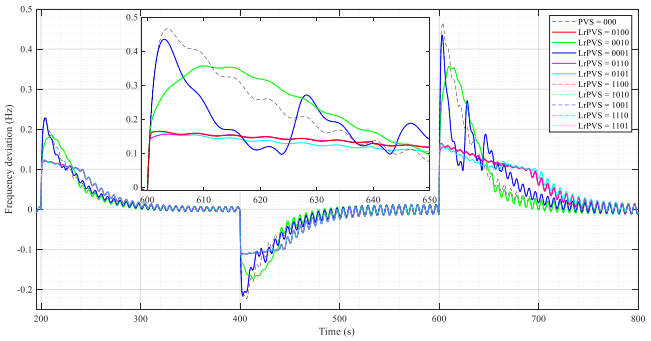

FIGURE 5. Frequency control performance under different events. Comparison between LR implementations. Control based on (13)**.**

on RMS (PVS = 101), is less sensitive to the implemented LR method. The control based on (11) provides smaller absolute maxima than the control based on (13).

TABLE 2. Performance metrics (mHz) of the curves of Fig. 4 and Fig. 5. The reference case (PVS = 000) is excluded.

FCP	Metrics	PVS = 100	PVS = 010	PVS = 001	PVS = 110	PVS = 101
Based on (11)	RMS(Δf) at Lr = 0	55.5267	74.1349	64.5939	55.5798	53.9000
	RMS(Δf) at Lr = 1	55.6994	71.7487	65.1451	55.7455	54.0781
	Max($\lvert\Delta f\rvert$) at Lr = 0	154.428	332.196	428.466	**149.106**	153.394
	Max($\lvert\Delta f\rvert$) at Lr = 1	154.835	336.164	428.735	150.313	153.795
Based on (13)	RMS(Δf) at Lr = 0	53.8384	72.5999	65.6310	53.8800	52.9655
	RMS(Δf) at Lr = 1	53.7636	72.6630	65.6882	53.7614	**52.8427**
	Max($\lvert\Delta f\rvert$) at Lr = 0	164.418	356.873	434.817	157.935	163.298
	Max($\lvert\Delta f\rvert$) at Lr = 1	163.940	355.019	435.046	157.486	162.843

2) Impact of the estimation of grid parameters on frequency control performance

The present section compares the impact on frequency control performance of using an ML-based DT or a perfect DT (initially denoted as Pt in Fig. 3). In this context, a perfect DT refers to a very well-known system, as stated in Section III-A, where it is possible to perfectly track every change over time on generators' dispatch. In Fig. 6 and Fig. 7 can be seen that colored dashed lines (Pt =1) almost fully coincide with continuous lines. Therefore, the proposed frequency controls, based on (11) and (13) are not sensitive enough to the deviations from the estimation of the power system coefficient. Again, the control based on (13) is even less sensitive. In Fig. 6, it is possible to observe small discrepancies in the standalone scenarios VI and SFC (PtPVS = Pt010 and PtPVS = Pt001).

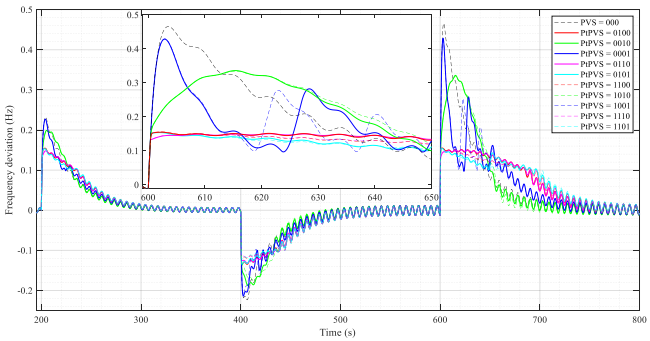

FIGURE 6. Frequency control performance under different events. Comparison between DT implementations. Control based on (11)**.**

Table 3 supports the fact that the frequency control based on (13) provides a smaller RMS and the control based on 11 smaller maxima. By comparing Table 2, it is noticeable that using ML-based DT can provide the same practical performance as a perfect DT-based frequency control.

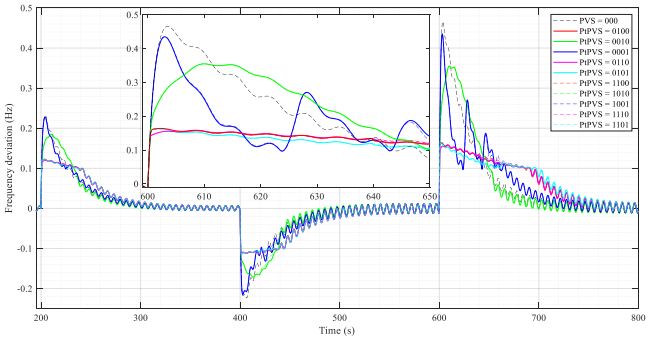

FIGURE 7. Frequency control performance under different events. Comparison between DT implementations. Control based on (13)**.**

TABLE 3. Performance metrics (mHz) of the curves of Fig. 6 and Fig. 7. Reference case (PVS = 000) is excluded.

FCP	Metrics	PVS = 100	PVS = 010	PVS = 001	PVS = 110	PVS = 101
Based on (11)	RMS(Δf) at Pt	54.4285	72.5677	65.0052	54.4377	53.3333
	Max($\lvert\Delta f\rvert$) at Pt	156.042	334.392	429.494	**149.927**	154.989
Based on (13)	RMS(Δf) at Pt	53.9954	72.3262	65.7206	54.0121	**53.0365**
	Max($\lvert\Delta f\rvert$) at Pt	162.672	354.934	435.710	156.406	161.636

3) Impact of the load dynamics on frequency control performance

As mentioned in Section II, the extent of the benefits of the loads may largely depend on their dynamics. Previous works (e.g., [24]) showed how frequency control improvements are limited due to the physical characteristics and operational restrictions on loads. This section evaluates the same previous frequency control schemes (Sections IV-A1 and IV-A2) but includes the HVAC system described in Section IV instead of an ideal load.

Fig. 8 repeats the tests in Fig. 2. Similarly, Fig. 9 and Fig. 10 repeat the setup of Fig. 4 and Fig. 5, respectively, at Lr = 1. As seen, the dynamics of the HVAC reach the stabilization around $t = 400\ s$. In contrast to an ideal load, this stabilization time slows the action of frequency controllers.

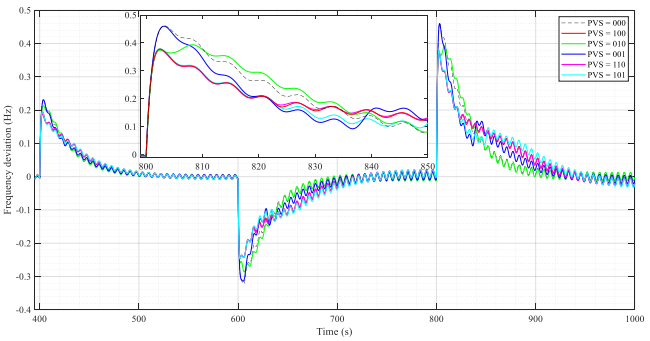

FIGURE 8. HVAC system impact on the frequency control performance under different events. Control based on (10)**.**

Table 4 exposes the control frequency performance based on (10). Due to the interaction of the HVAC system with generators, the reference case (PVS = 000) presents slightly different metrics. Furthermore, the degree of improvement is smaller than the one in Table 1. For instance, although combined controls perform the best (PVS =110 in max$\lvert\Delta f\rvert$ and PVS = 101 in RMS(Δf)), compared to Table 2, the improvement is not equally extensive.

Fig. 9 and Fig. 10 implement frequency controls based on (11) and (13), respectively. At first glance, it is evidenced that contrary to Sections IV-A1 and IV-A2, the difference among frequency control schemes is not highly noticeable. The combined controls (PVS = 110 and PVS = 101) still decrease the most the frequency deviation maxima.

Table 5 collects the metrics that describe the performance of Fig. 9 and Fig. 10. At least one of the frequency control

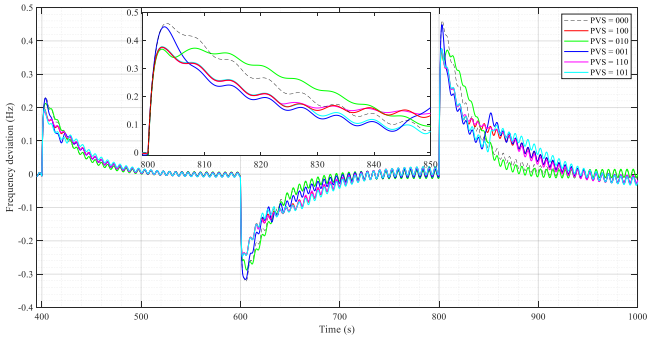

FIGURE 9. HVAC system impact on the frequency control performance under different events. Control based on (11)**.**

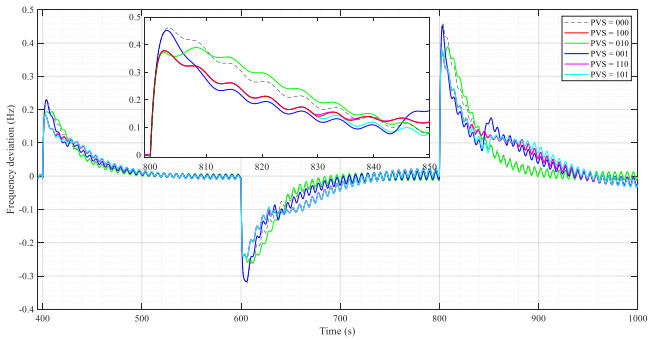

FIGURE 10. HVAC system impact on the frequency control performance under different events. Control based on (13)**.**

proposals exceeds the improvements obtained by classic standalone or combined controls (Table 4 and Fig. 8). The control based on (11) is still the best at reducing the max$\lvert\Delta f\rvert$ but with a standalone VI control (PVS = 010), not a combined control. The lowest RMS(Δf) is achieved by a combined frequency control (PVS = 101) with the control based on (13) but with a small difference compared to the standalone PFC based on (13). Although combined controls remain the best options, as well as both frequency control proposals based on (11) and (13), the improvement ratio between combined and standalone controls is reduced.

TABLE 4. Performance metrics (mHz) of the curves of Fig. 8.

Metrics	PVS = 000	PVS = 100	PVS = 010	PVS = 001	PVS = 110	PVS = 101
RMS(Δf)	80.1451	72.7142	79.5445	76.8769	72.7509	**72.3532**
Max($\lvert\Delta f\rvert$)	461.056	378.209	393.499	459.967	**375.854**	379.581

TABLE 5. Performance metrics (mHz) of the curves of Fig. 9 and Fig. 10. Reference case (PVS = 000) is excluded.

FCP	Metrics	PVS = 100	PVS = 010	PVS = 001	PVS = 110	PVS = 101
Based on (11)	RMS(Δf)	72.6629	80.3278	74.6392	72.8825	72.3184
	Max($\lvert\Delta f\rvert$)	376.000	**372.451**	448.707	373.840	377.474
Based on (13)	RMS(Δf)	72.2742	79.4732	74.9247	72.2700	**72.0978**
	Max($\lvert\Delta f\rvert$)	378.385	389.297	451.650	377.444	378.692

B. REAL-TIME EXPERIMENTAL VALIDATION

To properly assess the reliability of the proposals, real-time experimental validation is required. It is one of the most straightforward and reliable validation ways, as discussed in Section III-C. This experimental environment exposes the proposals to real noise, delays, and digital-to-analog / analog-to-digital conversion problems, among other challenges. Two HIL devices have been used for validation during asynchronous operation. The power system is modeled on a Typhoon HIL 402 and the load, along the power system DT, in an OP5700, from OPAL-RT. The time steps are 8 milliseconds and 2 milliseconds, respectively. Both HIL devices are connected to a main computer through a Local Area Network (LAN) in the PREDIS platform [56], and among them through coaxial to one-pin cables to exchange three analog signals. As seen in Fig. 11, the Typhoon HIL402 sends the frequency deviation signal through an analog output to the OP5700, and receives from it two analog signals, the load consumption and the probing signal.

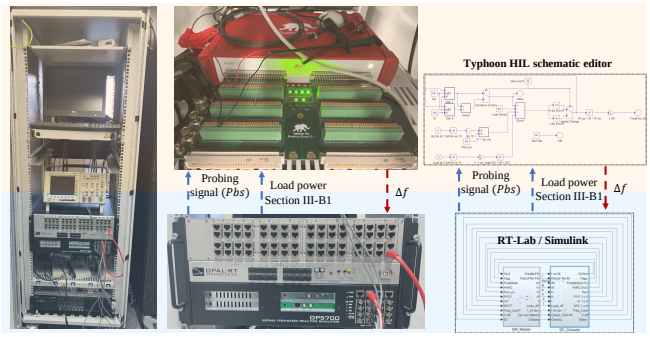

FIGURE 11. Experimental testbench. From left to right: board front side, Typhoon HIL 402 (at board back side) vs. OPAL-RT OP5700, and representative signal exchange between models (models loaded in the respective HIL device). The orange zone is the power system side. The blue zone is the load side. The color of the arrows represents the zone objective of signals.

Based on Section IV-A3, experimental validation focuses on the HVAC system. The differences between ideal load and HVAC results emphasize the need to test DT-based frequency control in HVAC settings. Additionally, a second-order band-pass filter is applied to the DT's analog input, tuned to the probing signal frequency in Section IV.

1) HVAC system frequency control performance

Taking into account the performance of the combined controls in Section IV-A, only one standalone control scheme, PVS = 100, is tested, in addition to the combined schemes. Across all the previous scenarios, the standalone SFC configuration (PVS = 001) resulted in the smallest improvement in Max($\lvert\Delta f\rvert$), while the standalone VI configuration (PVS = 010) yielded the least reduction in RMS(Δf). Fig. 12 shows the evolution of the frequency deviation after a sudden load loss. The HVAC system applies the frequency control based on (10). As seen, the stabilization time of the HVAC system, mentioned in Section IV-A3, should be considered to perform the tests, including between two consecutive tests. After load shedding, to gather relevant information, around 70 s are recorded. In this case, the combined frequency controls (PVS = 101 and 110) provided a larger reduction in maxima than the standalone control. Here, the performance in the reference case (PVS = 000) is RMS (f) = 109.245 mHz, and Max($\lvert f\rvert$) = 222.624 mHz.

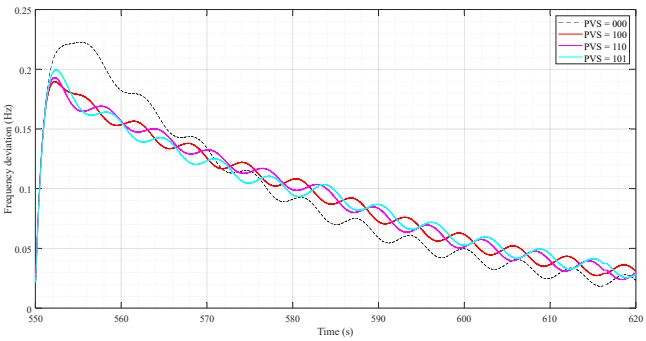

FIGURE 12. Laboratory test: HVAC system impact on the frequency control performance following a sudden load shedding. Control based on (10)**.**

Fig. 13 repeats the tests of Fig. 12 but implements the frequency control based on (11). At first sight, the degree of benefits compared to using the classic control based on (10) is

not extensive. Under this condition, the combined frequency controls perform better than the standalone scheme.

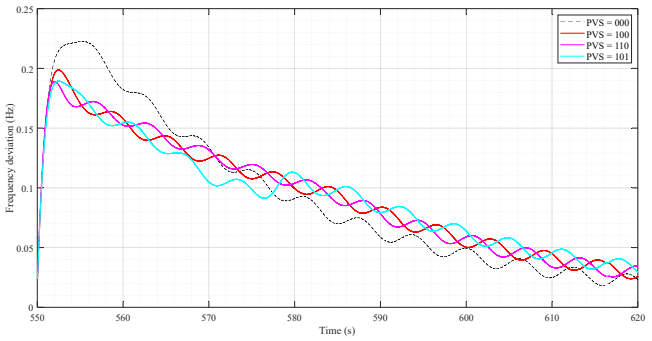

FIGURE 13. Laboratory test: HVAC system impact on the frequency control performance following a sudden load shedding. Control based on (11).

Fig. 14 shows the frequency performance under the implementation of the frequency control based on (13). At first glance, the degree of benefits is larger than in previous control schemes, mainly during the first seconds. Here, the combined controls are notably better than the standalone frequency control scheme.

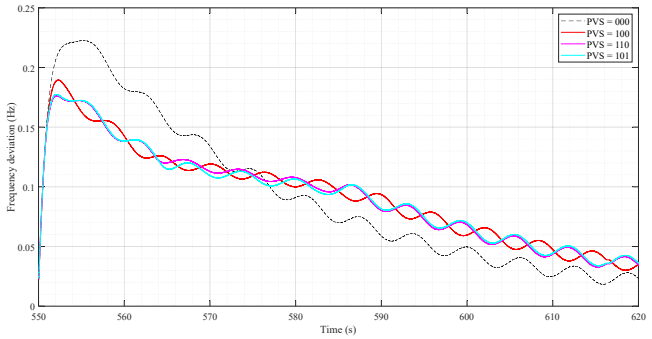

FIGURE 14. Laboratory test: HVAC system impact on the frequency control performance following a sudden load shedding. Control based on (13).

Table 6 collects the descriptive metrics selected to evaluate the frequency control performance. Contrary to the results in Section IV-A, the frequency control based on (13) provided the best metrics. The lowest maximum is obtained by the PVS = 110 control, which mixes PFC and VI. The lowest RMS is obtained with the PVS = 101 control, which mixes PFC and SFC. In any case, the DT-based frequency control proposals improved the power system frequency performance more than the frequency control solutions proposed by previous works.

TABLE 6. Performance metrics (mHz) of the curves of Fig. 12, Fig. 13, and Fig. 14. The reference case (PVS = 000) is excluded.

FCP	Metrics	PVS = 100	PVS = 110	PVS = 101
Based on (10)	RMS(Δf)	96.4357	97.6885	94.6231
	Max($\lvert\Delta f\rvert$)	189.583	193.034	199.479
Based on (11)	RMS(Δf)	97.123	96.4573	92.5667
	Max($\lvert\Delta f\rvert$)	198.698	188.965	189.388
Based on (13)	RMS(Δf)	91.4958	90.3814	**90.122**
	Max($\lvert\Delta f\rvert$)	189.355	**176.237**	177.441

C. DISCUSSION

This section gathers the tables of Section IV and compares each metric with the corresponding reference case (PVS = 000) of each table. This is 100(Metric/Reference - 1). Table 7 evidences that the control based on (11) provided the largest reduction in Max($\lvert\Delta f\rvert$) and the control based on (13) the largest reduction in RMS, in controls PVS = 110 and 101, respectively. Adding VI and SFC improved maxima reduction and RMS reduction, respectively. Coherently, the VI and SFC standalone controls only represent a certain degree of improvement in reducing maxima and RMS, respectively. Although combined controls performed the best, a PFC standalone control based on either of both frequency proposals is still better than any frequency scheme based on (10) (PVS = 101 with (10) is slightly better than PVS = 100 with (11)).

Table 8 summarizes the metrics obtained from Section IV-A3. At first glance, the degree of benefits decreased compared to the ideal load scenarios. However, some patterns remain: VI standalone and SFC standalone mainly contribute to the reduction of maxima and RMS, respectively; and the best improvements to maxima and RMS are PVS = 010 (followed by PVS = 110) with (11) and PVS = 101 with (13), respectively. In this scenario, the superiority of frequency control proposals over classic control based on (10) cannot be ensured by only the PFC standalone frequency control. In contrast to Table 7, the benefits of a standalone PFC control based on (11) or (13) are exceeded by three of the ten classic controls ((10) with PVS = 100, 110, and 101).

Table 9 collects the reference case referred metrics of Section IV-B1. In this scenario, the overall degree of improvement is higher than in Table 8. The control based on (13) is the best solution for both metrics, followed by the combined controls based on (11) (PVS = 101 with (10) is less than 2% better than PVS = 110 with (11)). In this experimental scenario, only any standalone PFC control based on (13) is better than any control based on (10). The controls based on (11) need to be combined among them to exceed any control based on (10).

As shown by the previous quantitative comparative results, both frequency control proposals enhance frequency performance. This improvement can be further amplified through the use of combined control strategies. Table 10 presents a qualitative summary of the key findings related to the frequency control approaches.

TABLE 7. Metrics percentual variation: the results of table 1, and table 2 compared to the reference case (PVS = 000).

FCP	Metrics	PVS = 100	PVS = 010	PVS = 001	PVS = 110	PVS = 101
Based on (10)	RMS(Δf)	-22.68	-1.13	-9.37	-22.71	-24.79
	Max($\lvert\Delta f\rvert$)	-57.51	-21.43	-4.36	-60.05	-57.82
Based on (11)	RMS(Δf)	-24.30	-2.48	-11.46	-24.23	-26.50
	Max($\lvert\Delta f\rvert$)	-66.76	-27.83	-7.96	**-67.73**	-66.98
Based on (13)	RMS(Δf)	-26.93	-1.24	-10.72	-26.93	**-28.18**
	Max($\lvert\Delta f\rvert$)	-64.81	-23.78	-6.60	-66.19	-65.04

TABLE 8. Metrics percentual variation: the results of table 4, and table 5 compared to the HVAC system reference case (PVS = 000).

FCP	Metrics	PVS = 100	PVS = 010	PVS = 001	PVS = 110	PVS = 101
Based on (10)	RMS(Δf)	-9.27	-0.75	-4.08	-9.23	-9.72
	Max($\lvert\Delta f\rvert$)	-17.97	-14.65	-0.24	-18.48	-17.67
Based on (11)	RMS(Δf)	-9.34	-0.23	-6.87	-9.06	-9.77
	Max($\lvert\Delta f\rvert$)	-18.45	**-19.22**	-2.68	-18.70	-18.13
Based on (13)	RMS(Δf)	-9.82	-0.84	-6.51	-9.83	**-10.04**
	Max($\lvert\Delta f\rvert$)	-17.93	-15.56	-2.04	-18.13	-17.86

TABLE 9. Metrics percentual variation: the results of table 6 compared to the HVAC system reference case (PVS = 000) in the laboratory tests.

FCP	Metrics	PVS = 100	PVS = 110	PVS = 101
Based on (10)	RMS(Δf)	-11.73	-10.58	-13.38
	Max($\lvert\Delta f\rvert$)	-14.84	-13.29	-10.40
Based on (11)	RMS(Δf)	-11.10	-11.71	-15.27
	Max($\lvert\Delta f\rvert$)	-10.75	-15.12	-14.93
Based on (13)	RMS(Δf)	-16.25	-17.27	**-17.50**
	Max($\lvert\Delta f\rvert$)	-14.94	**-20.84**	-20.30

TABLE 10. Qualitative assessment of the proposed frequency control methods.

Performance or implementation aspect	Comment
Reduction of RMS(Δf)	Owing to the use of constant gains, the proposal **based on** (13) achieved the greatest reduction.
Reduction of Max($\lvert\Delta f\rvert$)	As a result of gain tracking, the proposal **based on** (11) achieved the largest reduction.
Sensitivity to LR estimation deviations	Since it relies on LR estimation for further calculations, the proposal **based on** (13) was the least sensitive.
Performance under non-ideal load scenarios	Due to its lower sensitivity to biased or noisy inputs, the proposal **based on** (13) exhibited the best performance.
Initial condition requirements	Because gain tracking depends on expected values, the proposal **based on** (11) requires more accurate initial conditions.
Future condition requirements	As it assumes a predefined load event (in terms of type and magnitude) for further calculations, the proposal **based on** (13) requires more accurate forecasts of future conditions.
Scalability	**Both proposals** are potentially applicable to larger power systems. However, the previously mentioned requirements regarding initial and future conditions must be carefully addressed. In addition, under scenarios of high RG penetration and/or a diverse generation mix, complementary tools (e.g., probing signals, metering devices, and filtering techniques) must be properly designed to handle distorted measurements, high RoCoF, and controller interactions—among other emerging challenges. The proposal **based on** (13) may offer enhanced robustness in such conditions, as it is less sensitive to uncertainties and perturbations in the input signals.
Computational requirements	Due to the use of time-domain equations to predict extrema values, the proposal **based on** (13) demands greater computational capacity. This requirement also depends on the complexity of the equations implemented.

V. CONCLUSION

This work explores the role of loads in frequency control using Digital Twins. A novel framework integrates a Power System Digital Twin into load control schemes, leveraging gray-box models that combine data-driven and physics-based approaches. An extended linear regression method is introduced to estimate an equivalent integral term, enabling real-time monitoring of cumulative secondary frequency control contributions. Two frequency control schemes are proposed: one adjusts load responses based on inertia and control gains, while the other predicts deviations to optimize tuning.

Computational simulations and real-time experiments validate the approach. A multi-HIL test bench (OP5700 and Typhoon HIL 402) ensures heterogeneous and asynchronous conditions, demonstrating the framework's interoperability. Holistic validation improves reliability, though HIL testing should be carefully designed, as simulations run significantly faster than experiments (e.g., under test conditions of Section IV, the simulation is around 30 times faster than experimental validation).

In addition to an ideal load for assessing the proposals, a model of the HVAC system is considered. An adaptable air-refrigerant HVAC system is included in a railway thermal zone model. In doing this, the contribution of low thermal inertia loads is expanded. The main insights from the case studies of Section IV can be summarized as follows:

- The extended linear regression methods proposed can provide accurate tracking of real-time inertia, proportional gain, and integral gain. Especially the one based on (5), which is less sensitive to transients. Nonetheless, both possible implementations of LR forms provided practically the same frequency control performance.
- In all ideal load scenarios, either linear regression based on (4) or (5), the frequency control proposals, based on (11) and (13), provided better results than classical solutions based on (10) for the same frequency control scheme (i.e., PVS topology).
- In the scenario of a perfect Digital Twin, where there is no need for online estimation techniques, the frequency control performance is almost equal to the linear regression form based on (5). This fact shows the high tolerance of the frequency control proposals to possible uncertainties in the setpoints.
- The comparison of frequency control performance between an ideal load and HVAC system (Section IV-A3) shows that intrinsic dynamics and control loops affect the results. Although the HVAC system has a slower response, the overall trend remains, with the proposed controls outperforming classic solutions under the same scheme (PVS topology).
- In simulations, combined controls outperform standalone primary frequency control, simplifying Digital Twin and control requirements. In experiments, combined control is necessary to surpass classic controls. The most significant improvements are observed with the ideal load in simulation, followed by the HVAC system in experiments, and the HVAC system in simulation.

This study proposes an innovative application of Digital Twins to facilitate the integration of loads into ancillary service provision within power systems. The methodology is founded on precise system modeling and exploits the strengths of machine learning techniques to effectively manage system non-linearities and noise. Future research directions include extending the proposed framework to encompass a broader range of power system configurations, load models, frequency control mechanisms, and ancillary service categories, as well as exploring alternative Digital Twin architectures. Moreover, a comprehensive assessment of the approach's robustness is recommended under varying degrees of renewable generation penetration and diverse load conditions, accounting for the intrinsic dynamic behaviors of different generation and consumption technologies.

AUTHOR CONTRIBUTIONS

Author contributions according to Contributor Roles Taxonomy (CRediT): *Conceptualization:* J.A., A.L.; *Methodology:* J.A., A.L.; *Formal analysis:* J.A.; *Investigation:* J.A.; *Resources:* J.A., A.L.; *Data curation:* J.A.; *Writing - original draft:* J.A.; *Writing - review and editing:* J.A., A.L., Y.B., F.W., S.W., V.H.; *Visualization:* J.A.; *Supervision:* A.L., Y.B.,

F.W., S.W., V.H.; *Project administration:* A.L., Y.B., F.W., S.W., V.H.; *Funding acquisition:* A.L., Y.B., F.W., V.H.

REFERENCES

[1] IRENA, *Climate Action Support 2024*. Abu Dhabi: International Renewable Energy Agency, 2024.

[2] P. Denholm *et al.*, "The challenges of achieving a 100% renewable electricity system in the united states," *Joule*, vol. 5, pp. 1331–1352, 6 2021.

[3] J. Wachter, L. Gröll, and V. Hagenmeyer, "Survey of real-world grid incidents–opportunities, arising challenges and lessons learned for the future converter dominated power system," *IEEE Open Journal of Power Electronics*, vol. 5, pp. 50–69, 2024.

[4] J. Shair *et al.*, "Power system stability issues, classifications and research prospects in the context of high-penetration of renewables and power electronics," *Renewable and Sustainable Energy Reviews*, vol. 145, 7 2021.

[5] G. De Carne *et al.*, "The role of energy storage systems for a secure energy supply: A comprehensive review of system needs and technology solutions," *Electric Power Systems Research*, vol. 236, p. 110963, 2024. [Online]. Available: https://www.sciencedirect.com/science/article/pii/S0378779624008496

[6] N. Hatziargyriou *et al.*, "Definition and classification of power system stability - revisited & extended," *IEEE Transactions on Power Systems*, vol. 36, pp. 3271–3281, 7 2021.

[7] M. N. H. Shazon, Nahid-Al-Masood, and A. Jawad, "Frequency control challenges and potential countermeasures in future low-inertia power systems: A review," *Energy Reports*, vol. 8, pp. 6191–6219, 11 2022.

[8] R. Rajan, F. M. Fernandez, and Y. Yang, "Primary frequency control techniques for large-scale pv-integrated power systems: A review," *Renewable and Sustainable Energy Reviews*, vol. 144, p. 110998, 2021.

[9] D. Chong *et al.*, "Coordination optimization within large-scale virtual power plant for frequency stability improvement under internal power and external frequency fluctuations," *Applied Energy*, vol. 384, p. 125416, 2025.

[10] J. Boyle and T. Littler, "A review of frequency-control techniques for wind power stations to enable higher penetration of renewables onto the irish power system," *Energy Reports*, vol. 12, pp. 5567–5581, 2024.

[11] B. Loza *et al.*, "Grid-friendly integration of wind energy: A review of power forecasting and frequency control techniques," *Sustainability*, vol. 16, no. 21, 2024.

[12] S. Yumiki *et al.*, "Autonomous vehicle-to-grid design for provision of frequency control ancillary service and distribution voltage regulation," *Sustainable Energy, Grids and Networks*, vol. 30, p. 100664, 2022.

[13] M. Ledro *et al.*, "Influence of realistic ev fleet response with power and energy controllers in an ev-wind virtual power plant," *Sustainable Energy, Grids and Networks*, vol. 31, p. 100704, 2022.

[14] A. Blatiak *et al.*, "Value of optimal trip and charging scheduling of commercial electric vehicle fleets with vehicle-to-grid in future low inertia systems," *Sustainable Energy, Grids and Networks*, vol. 31, p. 100738, 2022.

[15] P. Bao, W. Zhang, and Y. Zhang, "Secondary frequency control considering optimized power support from virtual power plant containing aluminum smelter loads through vsc-hvdc link," *Journal of Modern Power Systems and Clean Energy*, vol. 11, no. 1, pp. 355–367, January 2023.

[16] International Energy Agency, "World energy outlook 2024," Paris, 2024, licence: CC BY 4.0 (report); CC BY NC SA 4.0 (Annex A). [Online]. Available: https://www.iea.org/reports/world-energy-outlook-2024

[17] F. Wurtz and B. Delinchant, ""Smart buildings" integrated in "smart grids": A key challenge for the energy transition by using physical models and optimization with a "human-in-the-loop" approach," *Comptes Rendus. Physique*, vol. 18, no. 7-8, pp. 428–444, 2017, wOS:000416698000008.

[18] Y. Lin *et al.*, "Experimental evaluation of frequency regulation from commercial building hvac systems," *IEEE Transactions on Smart Grid*, vol. 6, no. 2, pp. 776–783, March 2015.

[19] I. Beil, I. Hiskens, and S. Backhaus, "Frequency regulation from commercial building hvac demand response," *Proceedings of the IEEE*, vol. 104, no. 4, pp. 745–757, April 2016.

[20] M. Eissa *et al.*, "Emergency frequency control by using heavy thermal conditioning loads in commercial buildings at smart grids," *Electric Power Systems Research*, vol. 173, pp. 202–213, 2019.

[21] Y. Son *et al.*, "Hardware implementation and market impacts of grid-supportive functions in end-use loads," 3 2023.

[22] S. Subedi *et al.*, "Cost-benefit analysis of grid-supportive loads for fast frequency response," in *2023 IEEE PES Grid Edge Technologies Conference & Exposition (Grid Edge)*, 2023, pp. 1–5.

[23] J. Araúz and S. Martinez, "Contribution of the thermal inertia of trains to the primary frequency control of electric power systems," *Sustainable Energy, Grids and Networks*, vol. 34, p. 100988, 6 2023.

[24] ——, "Use of the thermal inertia of trains for contributing to primary frequency control and inertia of electric power systems," *IEEE Access*, vol. 11, pp. 57 099–57 116, 5 2023.

[25] ——, "Using the thermal inertia of trains for contributing to primary frequency control in grids with photovoltaic generation," in *2023 IEEE International Conference on Electrical Systems for Aircraft, Railway, Ship Propulsion and Road Vehicles & International Transportation Electrification Conference (ESARS-ITEC), Venice, Italy, 2023, pp. 1-6*. IEEE, 3 2023.

[26] ——, "Using the thermal inertia of trains for contributing to primary and supplementary frequency control in grids with high penetration of renewable generation," *IEEE ACCESS*, vol. 12, pp. 63 271–63 281, 5 2024.

[27] J. Araúz *et al.*, "Combined frequency control from trains thermal inertia: An assessment of frequency controllers interaction," *IEEE Open Journal of Power Electronics*, pp. 1–10, 3 2025.

[28] Z. He, C. Wan, and Y. Song, "Adaptive frequency response from electrified railway," *IEEE Transactions on Power Systems*, vol. 38, no. 3, pp. 2880–2894, May 2023.

[29] Y. Zhou *et al.*, "Digital twins for flexibility service provision from industrial energy systems," in *2021 IEEE 1st International Conference on Digital Twins and Parallel Intelligence (DTPI)*, July 2021, pp. 274–277.

[30] A. G. Abo-Khalil, "Digital twin real-time hybrid simulation platform for power system stability," *Case Studies in Thermal Engineering*, vol. 49, p. 103237, 2023.

[31] N. Kharlamova and S. Hashemi, "Evaluating machine-learning-based methods for modeling a digital twin of battery systems providing frequency regulation," *IEEE Systems Journal*, vol. 17, no. 2, pp. 2698–2708, June 2023.

[32] W. Li *et al.*, "A multi-purpose battery energy storage system using digital twin technology," *International Journal of Electrical Power & Energy Systems*, vol. 157, p. 109881, 2024.

[33] X. Chang *et al.*, "Frequency support coordinated control strategy of renewable distributed energy resource based on digital twins," *Electronics*, vol. 13, no. 17, 2024.

[34] J. Gao and H. Huang, "Stochastic optimization for energy economics and renewable sources management: A case study of solar energy in digital twin," *Solar Energy*, vol. 262, p. 111865, 2023.

[35] M. Pan *et al.*, "Real-time digital twin machine learning-based cost minimization model for renewable-based microgrids considering uncertainty," *Solar Energy*, vol. 250, pp. 355–367, 2023.

[36] W. Hua, B. Stephen, and D. C. Wallom, "Digital twin based reinforcement learning for extracting network structures and load patterns in planning and operation of distribution systems," *Applied Energy*, vol. 342, p. 121128, 2023.

[37] V. Nguyen *et al.*, "Digital twin integrated power-hardware-in-the-loop for the assessment of distributed renewable energy resources," *Electrical Engineering*, vol. 104, pp. 377–388, 2022.

[38] M. M. Zadeh *et al.*, "Development of real-time digital twins for particle accelerators," in *2024 Energy Conversion Congress & Expo Europe (ECCE Europe)*, Sep. 2024, pp. 1–5.

[39] N. Kofi Twum-Duah *et al.*, "Towards a Digital Twin of Grenoble-Presqu'île: A Framework for District-Scale Digital Twin Development," in *Conférence francophone de l'International Building Performance Simulation Association (IBPSA) 2024*, La rochelle, France, May 2024.

[40] A. E. Onile *et al.*, "Uses of the digital twins concept for energy services, intelligent recommendation systems, and demand side management: A review," *Energy Reports*, vol. 7, pp. 997–1015, 2021.

[41] P. Kundur, N. Balu, and M. Lauby, *Power System Stability and Control*, ser. EPRI power system engineering series. McGraw-Hill Education, 1994.

[42] N. Mohan, T. M. Undeland, and W. P. Robbins, *Power Electronics: converters, application, and design*, 3rd ed. John Wiley & Sons, Inc, 1997.

[43] IEEE Guide for Synchronous Generator Modeling Practices and Applications in Power System Stability Analyses. IEEE Std 1110-2002 (Revision of IEEE Std 1110-1991 [2003]): 1–72.

[44] "Recommended Practice for Excitation System Models for Power System Stability Studies," IEEE® Standard 421.5-1992, August, 1992.

[45] J. Araúz, "Contribution of railway systems to frequency control of electric power systems with a multidisciplinary approach," September 2024, thesis dissertation. [Online]. Available: https://oa.upm.es/83213/
[46] Y. Wang, A. Yokoyama, and J. Baba, "A multifunctional online estimation method for synchronous inertia of power systems using short-time phasor transient measurement data with linear least square method after disturbance," *IEEE Access*, vol. 12, pp. 17 010–17 022, 2024.
[47] N. E. Skopetou *et al.*, "Identification of inertia constants using time-domain vector fitting," *Electric Power Systems Research*, vol. 236, p. 110924, 2024. [Online]. Available: https://www.sciencedirect.com/science/article/pii/S0378779624008101
[48] J. Peng *et al.*, "Probing signal-based inertia and frequency response estimation for power systems with high levels of inverter-based resources," in *2024 IEEE Power & Energy Society General Meeting (PESGM)*, July 2024, pp. 1–5.
[49] L. Lavanya and K. S. Swarup, "Continuous real-time estimation of power system inertia using energy variations and q-learning," *IEEE Open Journal of Instrumentation and Measurement*, vol. 2, pp. 1–11, 2023.
[50] X. Deng *et al.*, "Pmu-based online inertia constant identification of the voltage source with inertia support to the grid," in *2024 International Conference on HVDC (HVDC)*, Aug 2024, pp. 660–663.
[51] J. D. Rios-Peñaloza *et al.*, "A two-stage online inertia estimation: Identification of primary frequency control parameters and regression-based inertia tracking," *Sustainable Energy, Grids and Networks*, vol. 40, p. 101561, 2024.
[52] N. Guruwacharya *et al.*, "Data-driven modeling of grid-forming inverter dynamics using power hardware-in-the-loop experimentation," *IEEE Access*, vol. 12, pp. 52 267–52 281, 2024.
[53] A. Arif *et al.*, "Load modeling—a review," *IEEE Transactions on Smart Grid*, vol. 9, no. 6, pp. 5986–5999, 2018.
[54] J. Geis-Schroer *et al.*, "Power-to-frequency dependency of residential loads in a wider frequency range: An experimental investigation," *IEEE Transactions on Industry Applications*, vol. 60, no. 6, pp. 9184–9194, Nov 2024.
[55] C. Vuik *et al.*, *Numerical Methods for Ordinary Differential Equations*. TU Delft OPEN Publishing, 2023.
[56] A. Labonne, "Méthodes et Outils pour la simulation et la validation expérimentale temps-réel des réseaux intelligents ou "Smart Grids"," Theses, Université Grenoble Alpes [2020-....], Nov. 2022. [Online]. Available: https://theses.hal.science/tel-03992940
[57] J. Rehrl and M. Horn, "Temperature control for hvac systems based on exact linearization and model predictive control," in *2011 IEEE International Conference on Control Applications (CCA)*, Sep. 2011, pp. 1119–1124.

JESÚS ARAÚZ received the M.S. degree in electrical engineering, and the Ph.D. degree in electrical and electronic engineering from the UPM, Madrid, Spain, in 2021 and 2024, respectively. His research interests are railway systems, building energy performance, integration of renewable generation in low-inertia grids, demand response, and ancillary services in power systems.

ANTOINE LABONNE is responsible of Distributed Energy Platform and facilities of G2Elab/ENSE3. He received his M.S. degree in mechatronics from the University of Blaise Pascal, Aubiere, France, in 2005, and the Electrical Engineering Diploma from the Grenoble Institute of Technology, Grenoble, France. Since 2005, he has been an Engineer at Grenoble INP doing his research at the G2Elab. His research interests have concerned the electricity network field, energy production systems, and renewable energy integration. In 2022, he received a Ph.D. degree from Grenoble Alpes University. His research interests are interoperability and SCADA-as-a-service, holistic validation of cyber-physical energy systems, and hardware-in-the-loop dedicated to energy systems.

YVON BESANGER (Senior Member, IEEE) received the Ph.D. degree in electrical engineering from the Grenoble INP, in 1996. He is currently a Professor with the ENSE3, Engineers' School for Water, Energy and Environment Sciences, and the Grenoble Electrical Engineering Laboratory. His research interests include the distribution networks' operation and reliability, blackout prevention, power system security, and interoperability in smart grids.

FREDERIC WURTZ (Member, IEEE) was born in France in 1970. He received the M.S. degree in electrical engineering and the Ph.D. degree from the Grenoble Institute of Technology (Grenoble INP), Grenoble, France, in 1993 and 1996, respectively. He has been a CNRS Senior Researcher, developing his research program with the Grenoble Electrical Engineering Laboratory since 1998. His research interests include the process design of electromagnetic devices, as well as the development of methods and tools in this area. In last years, he has extended new interests in complete system design of energy management for cars, planes, smart buildings, and smart grids with an interdisciplinary approach from engineering to social science.

SIMON WACZOWICZ received the Ph.D. degree in mechanical engineering from KIT in 2018. Since then, he has headed the Research Platform Energy department at the IAI at KIT. His research interests include energy system design and operation, and time series analysis and forecasting.

VEIT HAGENMEYER received the Ph.D. degree from Université Paris XI, Paris, France, in 2002. He is currently a Professor of Energy Informatics with the Faculty of Computer Science, and the Director of the IAI at KIT. His research interests include modeling, optimization and control of sector-integrated energy systems.